JARQ 60 (4), 399-407 (2026) https://www.jircas.go.jp

Identification of Neon Flying Squid (*Ommastrephes bartramii*) Fishing Grounds through 3D Water-Temperature Analysis

Daichi SUZUKI[1]*, Takayoshi OTAKI[2], Mitsuo SAKAI[3] and Yoshiki KATO[1]

[1] Marine Fisheries Research and Development Center, Japan Fisheries Research and Education Agency, Yokohama, Japan
[2] Japan Fisheries Information Service Center, Tokyo, Japan
[3] Ministry of Marine Affairs and Fisheries of Indonesia, Jakarta, Indonesia

Abstract

This study investigated the factors influencing the formation of fishing grounds for the neon flying squid (*Ommastrephes bartramii*), whose importance has increased due to the recent decline in Japanese common squid (*Todarodes pacificus*) resources since around 2015–2016. Using catch data from squid jigging vessels operating from May to July between 2019 and 2022, together with oceanographic data from the Hybrid Coordinate Ocean Model (HYCOM), we analyzed the three-dimensional (3D) temperature structure of *O. bartramii* habitat. Kernel density estimation was applied to characterize temperature distributions and to quantify the presence or absence of thermal frontal structures at specific temperatures. A generalized linear mixed model was then used to examine the relationship between these thermal fronts and catch per unit effort. The results indicated that the presence of frontal structures at 8°C-10°C in May, 8°C in June, and 6°C-10°C in July was associated with increased catches. These findings suggest that not only surface temperatures, but also intermediate-water thermal gradients play an important role in the formation of *O. bartramii* fishing grounds and that incorporating 3D environmental information could improve the accuracy of fishing-ground prediction models.

Discipline: Fisheries
Additional key words: squid jigging

Introduction

In Japan, the neon flying squid (*Ommastrephes bartramii*) is an important fishery resource (Fisheries Agency & Fisheries Research and Education Agency 2024), especially in light of the recent decline in Japanese common squid (*Todarodes pacificus*) resources since around 2015-2016 (Miyahara et al. 2025, Okamoto et al. 2025). The species is widely distributed in the North Pacific across subtropical and subarctic regions (Roper et al. 1984). It is known to hatch in subtropical spawning grounds and migrate to subarctic foraging grounds (Murata et al. 1988; Murata et al. 1998; Ichii et al. 2009; Kato et al. 2014, 2015). Two seasonal cohorts are recognized: autumn-spawning and winter–spring-spawning (Ichii et al. 2009). From May to July, Japan's squid jigging vessels mainly harvest the autumn-spawning cohort that has newly populated the foraging grounds (Fisheries Agency & Fisheries Research and Education Agency 2024) (Fig. 1).

Recent long-term analyses show that, from April to August, the summer habitat and fishing grounds of *O. bartramii* shift northward and converge on the Subarctic Frontal Zone around 40-43°N (Kato et al. 2023). This front likely offers an optimal combination of temperature and prey availability for the species (Kato et al. 2023). Given the broad habitat range with north–south migration, it has been difficult to estimate the location and extent of fishing grounds with high confidence. A habitat forecasting model based on oceanographic conditions has been practically applied to *O. bartramii* (Igarashi et al. 2011), contributing to efficient searches for fishing grounds. However, current models are point-estimate models that do not explicitly consider spatial structure, whereas fishers take water temperature within a certain surrounding area into account when choosing a fishing

*Corresponding author: suzuki_daichi86@fra.go.jp
Received 3 December 2025; accepted 2 March 2026; J-STAGE Advanced Epub 30 July 2026.
https://doi.org/10.6090/jarq.24S29

ground. Operational practices and behavioral ecology also indicate the importance of evaluating vertical water structure. In daytime squid jigging, jigs are typically lowered to approximately 300 m-330 m, and vertical migration based on biotelemetry has reported dives to about 350 m for autumn-spawning cohorts during foraging migrations (Sakai et al. 2006, Sakai et al. 2012). Accordingly, this study focused on the surface and a depth of 350 m as key behavioral layers, and evaluated fishing grounds in three dimensions within the May-July season. Based on these considerations, we examined whether three-dimensional (3D) thermal structure influences fishing-ground formation.

Materials

1. Catch data

We used catch and position data from May to July during 2019-2022, collected from 38 squid jigging vessels. Of these, 37 vessels were equipped with approximately 26 automatic jigging machines, while one larger vessel was equipped with 52 machines. Operating hours varied daily. For *O. bartramii* operations, fishing occurred during both daytime and nighttime periods, and catch and position data were recorded separately for day and night, with catch expressed as case counts. Because precise estimation of a vessel's daily operating hours is difficult, we assumed equal daily operating time. Accordingly, we treated the number of automatic jigging machines as effort, and defined the catch per unit effort (CPUE) as the number of cases per automatic jigging machine.

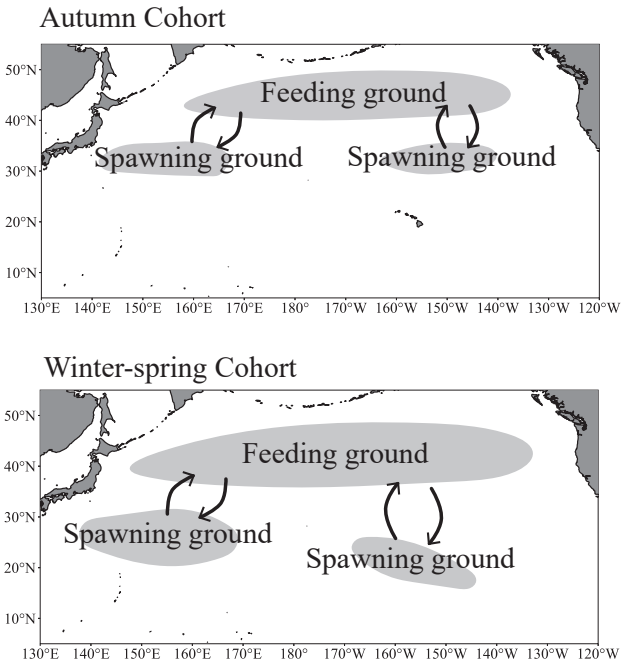


Fig. 1. Migration patterns of the autumn and winter-spring cohorts of *O. bartramii*

2. Ocean data

Ocean data were obtained from the Hybrid Coordinate Ocean Model (HYCOM) developed by the U.S. Naval Research Laboratory. Specifically, we extracted daily temperatures from 0 to 400 m using the Global Ocean Forecasting System 3.1 output on the GLBy0.08 grid for 2019-2022. We also extracted daily sea surface height (SSH) and sea surface salinity (SSS) from the same system. The HYCOM horizontal resolution is 1/12° × 1/12°.

Methods

1. Capturing 3D temperature distributions using KDE

We performed a kernel density estimation (KDE; Silverman 1986, Worton 1989) by year and month for water temperatures at the surface and a depth of 350 m at each catch location to characterize the distributional shape.

For univariate temperature KDE with the observed temperature series expressed as $\{T_i\}_{i=1}^{n}$, the density estimate at temperature t is given by

$$\hat{f}(t) = \frac{1}{nh}\sum_{i=1}^{n} K\left(\frac{t - T_i}{h}\right). \quad (1)$$

Here, n denotes the sample size, h the bandwidth, and K the kernel function. We used the Gaussian kernel:

$$K(u) = \frac{1}{\sqrt{2\pi}}\exp\left(-\frac{u^2}{2}\right), \quad u = \frac{t - T_i}{h}. \quad (2)$$

2. Identifying high-use locations via latitude–longitude KDE and constructing north–south temperature sections

The temperature ranges used for analysis were defined based on the KDE-derived temperature distributions.

$$\Theta = \{4, 6, 8, 10, 12\}℃ \quad (3)$$

By year and by month, we applied a bivariate KDE to catch locations in latitude φ and longitude λ to identify high-use fishing locations. For observation coordinates $\{\varphi_i, \lambda_i\}_{i=1}^{n}$, the density estimate at evaluation point (φ, λ) is defined as

$$\hat{f}(\varphi,\lambda)=\frac{1}{nh_\varphi h_\lambda}\sum_{i=1}^{n}K\left(\frac{\varphi-\varphi_i}{h_\varphi}\right)K\left(\frac{\lambda-\lambda_i}{h_\lambda}\right). \quad (4)$$

We also constructed north–south temperature sections from monthly mean temperatures. For each $\theta \in \Theta$ and latitude φ, the depth in meters at which that temperature occurs is defined as $z(\theta,\varphi)$, within the range 0 m-400 m. If no value exists within ± 0.5°C of the target temperature, the datum was treated as missing.

3. Definition of "frontal structure (present/absent)"

Let the latitude of the catch location be φ_0, and the step size be $\Delta_\varphi = 0.5°$. Then, the slope and curvature by central differences are defined as follows:

$$slope_{catch}(\theta,\varphi_0)=\frac{z(\theta,\varphi_0+\Delta_\varphi)-z(\theta,\varphi_0-\Delta_\varphi)}{2\Delta_\varphi} \quad (5)$$

$$curv_{catch}(\theta,\varphi_0)=\frac{z(\theta,\varphi_0+\Delta_\varphi)-2z(\theta,\varphi_0)+z(\theta,\varphi_0-\Delta_\varphi)}{(\Delta_\varphi)^2} \quad (6)$$

For the northern evaluation point (north), let $\varphi_1=\varphi_0+1°$, and compute the slope and curvature by substituting φ_0 with φ_1 in the above (catch) formulas.

Next, for each $\theta \in \Theta$, we defined a binary index B_θ (present = 1, absent = 0) using the following decision rule:

$$B_\theta=\begin{cases}\text{if } \begin{array}{c}|\,slope_{\text{north}}(\theta,\varphi_1)\,|\;>\;|\,slope_{\text{catch}}(\theta,\varphi_0)\,|\\ \text{and } |\,curv_{\text{north}}(\theta,\varphi_1)\,|\;>\;|\,curv_{\text{catch}}(\theta,\varphi_0)\,|\end{array}\\ \text{otherwise}\end{cases} \quad (7)$$

4. Statistical analysis (GLMMs)

Using, as explanatory variables, the presence/absence (1/0) of frontal structures at specific temperatures (4, 6, 8, 10, and 12°C) defined in increments of 2°C, we fitted independent generalized linear mixed models (GLMMs; Bolker et al. 2009) including Month (May, June, and July) and Month × frontal structure interactions. The response variable was catch (number of cases), with effort (number of machines) included as an offset, that is, log(effort). SSH and SSS were additionally included as covariates. Random intercepts were included for the vessel, day, and year. The GLMMs were implemented with R (version 4.2.2).

For observation i in each month, the model is given by

$$\begin{aligned}Y_i &\sim Poisson(\mu_i),\\ \eta_i &= \log\mu_i\\ &= \beta_0+\sum_{\theta\in\{6,8,10,12\}}\gamma_\theta B_{\theta.i}\\ &+\sum_{\theta\in\{4,6,8,10,12\}}\delta_{\theta,Month[i]}B_{\theta.i}+\alpha_1 SSH_i+\alpha_2 SSS_i\\ &+b_{\text{vessel}[j(i)]}+b_{\text{day}[d(i)]}+b_{\text{year}[y(i)]}\\ &+log(effort_i). \end{aligned} \quad (8)$$

Here, Y_i denotes the catch for observation$i$, μ_i is the expected value, and $B_{\theta,i}$ indicates the presence/absence (1/0) of frontal structure at θ ℃. $b_{\text{vessel}[j(i)]}$, $b_{\text{day}[d(i)]}$ and $b_{\text{year}[y(i)]}$ account for vessel, day, and year specific deviations.

Results

1. Analysis of fishing-ground temperatures

The KDE-derived peak temperature of surface water at the fishing grounds yielded 13.64°C in May, 13.45°C in June, and 13.64°C in July, indicating little monthly variation (Fig. 2). At a depth of 350 m, the KDE value decreased over time: 8.36°C in May, 7.27°C in June, and 6.55°C in July. Temperature ranges also shifted lower with season: May, 6°C-12°C; June, 5°C-12°C; and July, 4°C-8°C.

2. Thermal environment around catch locations

From the spatial KDE, high-frequency catch locations shifted northward from May to July in each year (Fig. 3; Table 1). The centers of the fishing grounds were located around 38° N in May and moved to approximately 44° N in July. Longitudinal positions varied considerably among years without a consistent 3D pattern. In meridional temperature sections at these locations (red crosses in Figure 3), abrupt shoaling of isotherms with northward movement was observed in several months, particularly in May, June, and July 2019; June 2020; June and July 2021; and May, June, and July 2022 (Fig. 4).

3. Statistical analysis

The results for the GLMMs are summarized in Table 2. Effects of frontal structures differed by month (Month × frontal structure), after accounting for sea surface height (SSH) and surface salinity (SSS) and including random intercepts for vessel, day, and year. In May, the presence of the 8°C and 10°C frontal structures

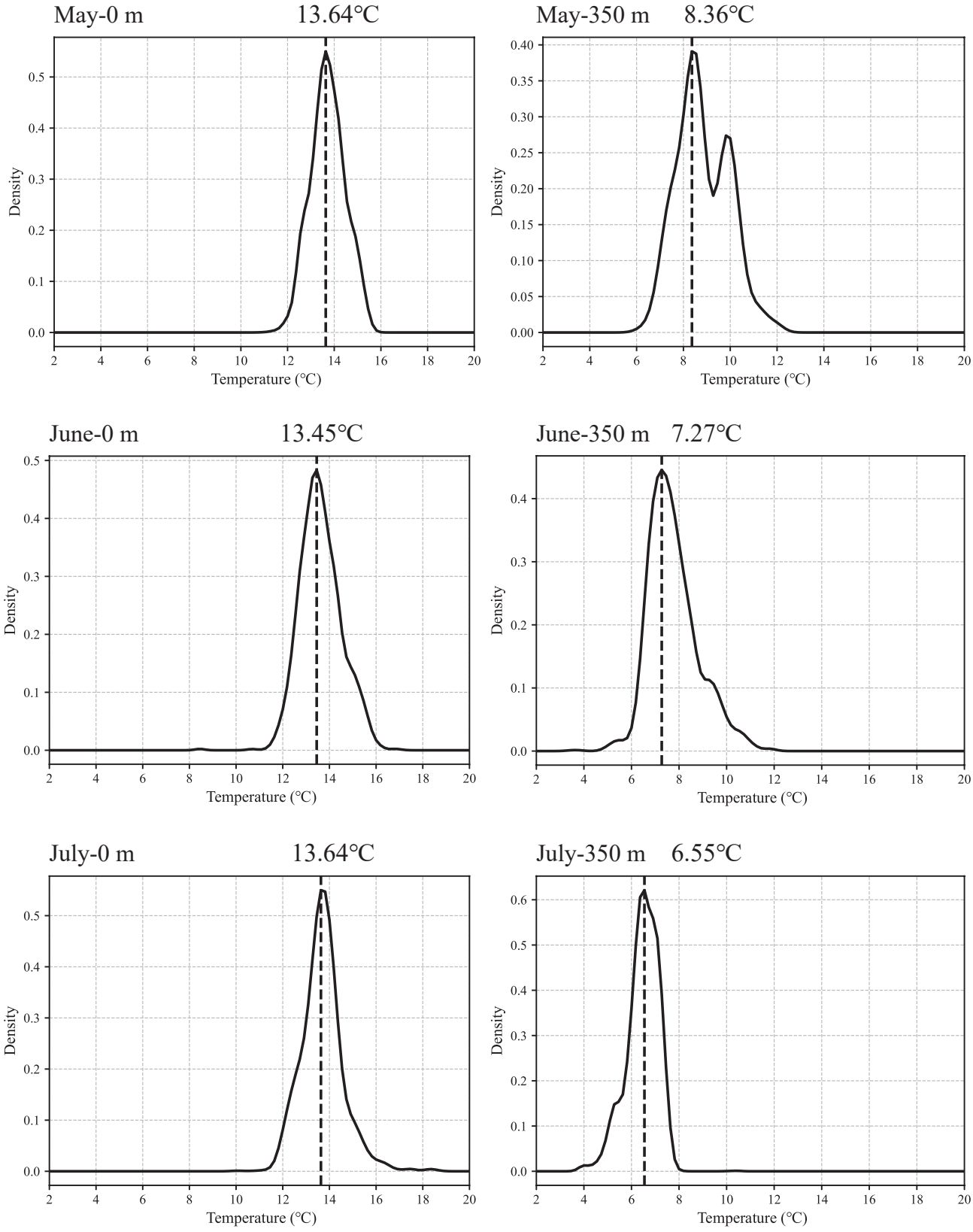


Fig. 2. KDE analysis results for water temperatures at the surface and a depth of 350 m in *O. bartramii* fishing grounds during May-July

The broken line indicates KDE density, and the dotted line indicates the KDE-derived peak temperature.

was associated with significantly higher catch (8°C: IRR = 1.073, $p < 0.001$; 10°C: IRR = 1.087, $p < 0.001$), whereas the 12°C frontal structure showed a significant negative effect (IRR = 0.919, $p < 0.001$) and the 6°C frontal structure was not significant. In June, only the 8°C frontal structure showed a significant positive effect (IRR = 1.041, $p < 0.001$), while the 6°C, 10°C, and 12°C frontal structures were not significant. In July, the 6°C and 10°C frontal structures had significant positive effects (6°C: IRR = 1.017, $p < 0.05$; 10°C: IRR = 1.020, $p < 0.05$), whereas the 8°C and 12°C frontal structures had significant negative effects (8°C: IRR = 0.963, $p < 0.001$; 12°C: IRR = 0.922, $p < 0.001$). SSH and SSS showed significant positive effects in the model (both $p < 0.001$). The 4°C frontal structure was excluded from the final analysis because its presence was extremely rare, leading to unstable estimation. Overall, the temperature range exhibiting positive effects varied seasonally: positive effects were centred around 8°C-10°C in May, concentrated at 8°C in June, and extended to 6°C (while remaining at 10°C) in July.

Discussion

The temperature at a depth of 350 m at fishing locations decreased from May through July, whereas the surface temperature changed little. This may reflect fishers' reliance on surface temperature when initiating fishing operations. *O. bartramii* fishing grounds tend to form on the northeastern sides of warm-core eddies (Igarashi et al. 2011, Alabia et al. 2015), where meridional temperature fronts can develop—as seen near 38° N, 177° W in May 2019 and near 40° N, 177° E in June 2019. However, fishing grounds also sometimes formed in months without clearly defined warm-core eddies. The GLMMs showed that the temperatures at which frontal structures increased the catch differed by month; thus, using the month-specific presence of such structures as indicators can contribute to increased catch. Specifically, in May, the presence of the 8°C and 10°C frontal structures was beneficial; in June, only the presence of the 8°C frontal structure was beneficial; and in July, the presence of the 8°C frontal structure was no longer beneficial, whereas the presence of the 10°C or 6°C frontal structure became beneficial. Although the 10°C effect was absent in June, it re-emerged in July. Note that, in July 2019, while a frontal structure appears south of the high-frequency location, meridional sections from 2020 to 2022 show the 10°C isotherm around ~50 m regardless of latitude, implying that a clear front seldom formed; thus, the 10°C frontal structure in July is unlikely to serve as a practical indicator. Previous behavioral and physiological studies have demonstrated that water temperature strongly affects the squid distribution and catch success for *O. bartramii* (Chen et al. 2010, Vijai et al. 2015, Wang et al. 2021). Embryonic development proceeds at 18°C-25°C (optimum 21°C-25°C), whereas growth occurs across a wide range of 5°C-27°C, and the preferred surface temperatures are 11°C-19°C, with higher catchability at 15°C-19°C. These findings indicate that thermal tolerance differs depending on the squid life stage, and that latitudinal cooling encountered during northward migration may impose environmental constraints on movement and distribution. In the autumn-spawning cohort, sex-specific migration and distribution have been suggested: females continue migrating northward into higher-latitude foraging grounds as they grow, whereas males tend to remain farther south and return south earlier than females (Bower & Ichii 2005, Ichii et al. 2009). In addition, large individuals in the foraging grounds of the autumn cohort are reported to be predominantly female (Chen 2010), implying that the catch in our study area may have been female-biased. Therefore, the effects of frontal structures and temperature estimated by the GLMMs may primarily reflect the distributional characteristics of females within the autumn cohort, and caution is warranted when generalizing our results to the entire autumn cohort, particularly males. As noted above, fishing grounds were often located immediately south of thermal fronts, suggesting that individuals tend to remain on the warmer side. This pattern can be interpreted primarily as a consequence of thermal constraints on further northward movement. Oceanic fronts can also enhance local prey availability and foraging opportunities for pelagic consumers (Polovina et al. 2001). *O. bartramii* is known to feed on micronektonic organisms in the transitional region of the North Pacific (Watanabe et al. 2004), and prey-related processes may therefore contribute to localized aggregations near frontal structures. Nevertheless, in our study, the temperature range of frontal-structure indicators associated with increased catch shifted seasonally from 10°C in May to 6°C-8°C in

Table 1. KDE-derived latitudes of high-use fishing locations by month

Year	*May*	*June*	*July*
2019	38° 15′ N	39° 30′ N	40° 47′ N
2020	39° 32′ N	40° 44′ N	42° 13′ N
2021	39° 59′ N	40° 37′ N	41° 47′ N
2022	39° 30′ N	40° 44′ N	43° 54′ N

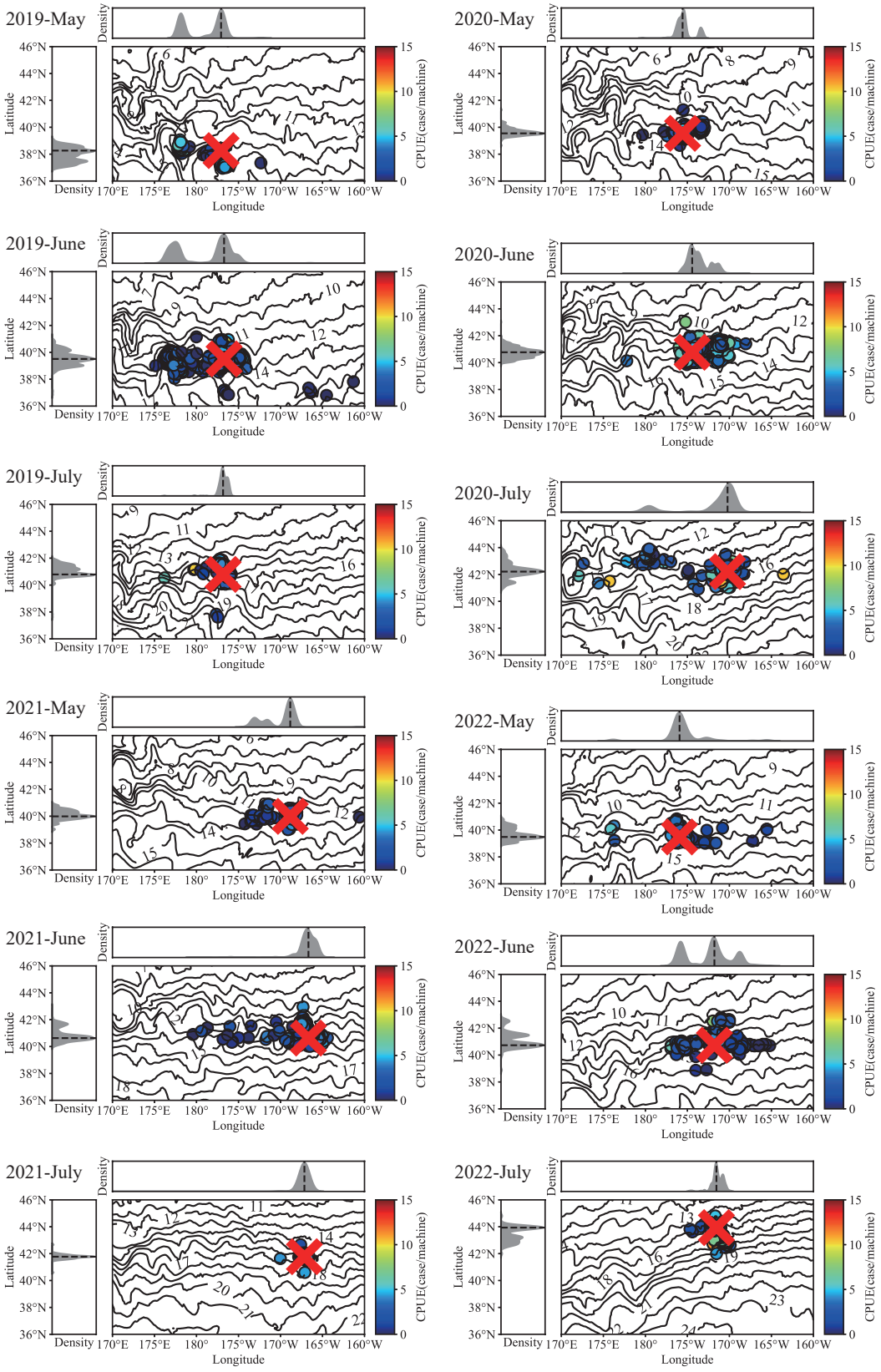


Fig. 3. KDE analysis results for the latitude and longitude of fishing locations, and distribution map of CPUE by year and month

In each panel, the graph on the left shows the KDE analysis results for latitude, the upper graph shows the KDE results for longitude, and the center graph plots the CPUE against the average surface water temperature.

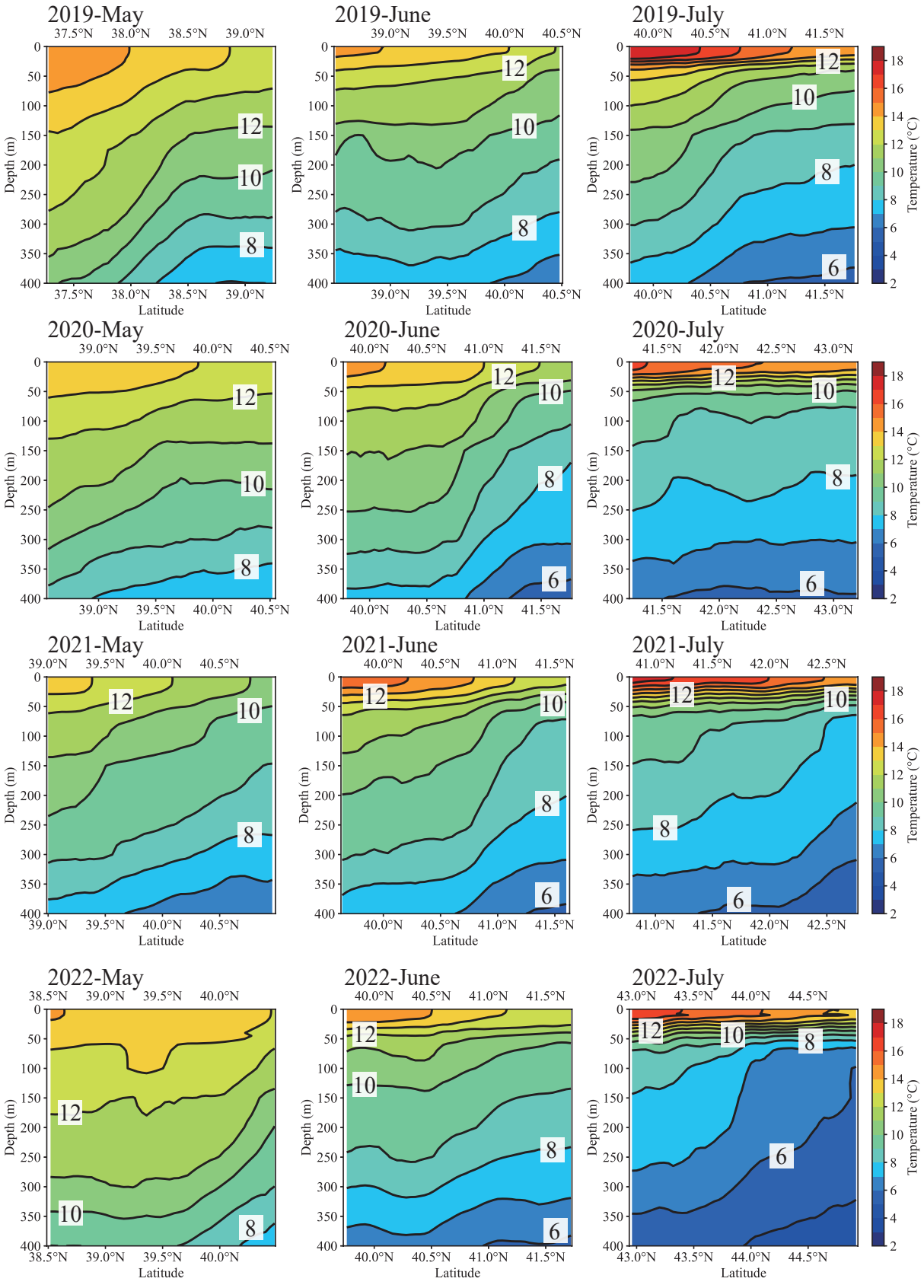


Fig. 4. North–south water temperature cross sections down to a depth of 400 m, centered on high-use fishing locations identified by KDE analysis

Table 2. GLMM Results

Month	Variable	Estimate	Std. Error	z-value	*p*-value		IRR
May	*12℃ Frontal structure*	–0.08413	0.02323	–3.62160	3 E–04	***	0.92
May	*10℃ Frontal structure*	0.08343	0.01135	7.35055	2 E–13	***	1.09
May	*8℃ Frontal structure*	0.07026	0.01176	5.97749	2 E–09	***	1.07
May	*6℃ Frontal structure*	0.00674	0.02427	0.27784	8 E–01	ns	1.01
June	*12℃ Frontal structure*	0.00985	0.01118	0.88041	4 E–01	ns	1.01
June	*10℃ Frontal structure*	–0.00460	0.00521	–0.88308	4 E–01	ns	1.00
June	*8℃ Frontal structure*	0.04035	0.00443	9.10225	9 E–20	***	1.04
June	*6℃ Frontal structure*	0.00399	0.00585	0.68192	5 E–01	ns	1.00
July	*12℃ Frontal structure*	–0.08089	0.01394	–5.80325	7 E–09	***	0.92
July	*10℃ Frontal structure*	0.02008	0.00996	2.01574	4 E–02	*	1.02
July	*8℃ Frontal structure*	–0.03734	0.00822	–4.54148	6 E–06	***	0.96
July	*6℃ Frontal structure*	0.01718	0.00780	2.20192	3 E–02	*	1.02
All (May-July)	*SSH*	0.41104	0.03784	10.86257	2 E–27	***	1.51
All (May-July)	*SSS*	0.16011	0.01911	8.37770	5 E–17	***	1.17

July, which is consistent with a seasonal shift in the effective thermal front. Accordingly, seasonality should be considered when applying these indicators. Such squid aggregations along the frontal structures form transient, temperature-dependent fishing grounds.

In summary, viable indicators appear to be the presence of the 10°C and 8°C frontal structures in May, the presence of the 8°C frontal structure in June, and the presence of the 6°C frontal structure in July. Incorporating month-varying frontal structure presence, in addition to point-based habitat forecasts, should improve the prediction of fishing grounds. However, although the present study analyzed data on a monthly basis, the northward migration of *O. bartramii* actually occurs as a continuous process; thus, the frontal structures serving as indicators likely shift gradually over time.

Acknowledgements

The authors thank the chief fishermen of the squid-jigging vessels who provided the data used in this study. We also thank Dr. Shitamitsu for proposing the research idea. Finally, we appreciate the valuable comments provided by the anonymous reviewers.

References

Alabia, I. et al. (2015) Identifying pelagic habitat hotspots of Neon flying squid in the temperate waters of the central North Pacific. *PLoS One*, **10**, e0142885. https://doi.org/10.1371/journal.pone.0142885.

Bolker, B. M. et al. (2009) Generalized linear mixed models: a practical guide for ecology and evolution. *Trends Ecol. Evol.*, **24**, 127-135.

Bower, J. R. & Ichii, T. (2005) The red flying squid (*Ommastrephes bartramii*): A review of recent research and the fishery in Japan. *Fish. Res.*, **76**, 39-55.

Chen, C. S. (2010) Abundance trends of two neon flying squid (*Ommastrephes bartramii*) stocks in the North Pacific. *ICES J. Mar. Sci.*, **67**, 1336-1345.

Chen, X. et al. (2010) A modeling approach to identify optimal habitat and suitable fishing grounds for neon flying squid (*Ommastrephes bartramii*) in the Northwest Pacific Ocean. *Fish. Bull.*, **108**, 1-14.

Fisheries Agency & Fisheries Research and Education Agency (2024) Neon flying squid in the North Pacific. *Kokusai gyogyo shigen no genkyo* (*Current Status of International*

Fishery Resources). https://www.kokushi.fra.go.jp/R06/R06_70_OFJ.pdf. Accessed on 4 December 2025 [In Japanese].

Ichii, T. et al. (2009) Life history of the neon flying squid: effect of the oceanographic regime in the North Pacific Ocean. *Mar. Ecol. Prog. Ser.*, **378**, 1-11.

Igarashi, H. et al. (2011) A statistical approach to identify optimal habitat suitability of neon flying squid in northwestern North Pacific by using satellite datasets and 3-D ocean data assimilation product. *Proc. PICES 2011 Annu. Meet.*, Khabarovsk, Russia, 36 pp.

Kato, Y. et al. (2014) Effects of hydrographic conditions on the transport of neon flying squid *Ommastrephes bartramii* larvae in the North Pacific Ocean. *Hidrobiológica*, **24**, 33-38.

Kato, Y. et al. (2015) Stable isotope analysis of gladius to investigate migration and trophic patterns of the neon flying squid (*Ommastrephes bartramii*). *Fish. Res.*, **173**, 169-174.

Kato, Y. et al. (2023) Summer habitat and fishing ground of *Ommastrephes bartramii* related with the North Pacific Subarctic Frontal Zone using long-term field research data. *JARQ*, **57**, 145-152.

Metzger, E. J. et al. (2017) Global Ocean Forecast System 3.1: Description and evaluation. *Naval Research Laboratory Memorandum Report RL/MR/7320-17-9722*, 72 pp.

Miyahara, T. et al. (2025) Stock assessment and evaluation for Japanese common squid (autumn-spawning cohort) (fiscal year 2025). *Marine fisheries stock assessment and evaluation for Japanese waters*. Japan Fisheries Agency and Japan Fisheries Research and Education Agency, Tokyo, 81 pp. https://www.fra.go.jp/shigen/fisheries_resources/meeting/ stock_assessment_meeting/2025/files/sa2025-sc16/fra-sa2025-sc16-02.pdf. Accessed on 12 February 2026 [In Japanese].

Murata, M. et al. (1988) Some biological aspects of neon flying squid *Ommastrephes bartramii* caught by Japanese squid gillnetters in the North Pacific. *Bull. Int. North Pac. Fish. Comm.*, **47**, 13-27.

Murata, M. et al. (1998) Seasonal migration and diel vertical migration of the neon flying squid, *Ommastrephes bartramii*, in the North Pacific. In Okutani, T. (ed.), *Contributed Papers to International Symposium on Large Pelagic Squids*. Japan Marine Fishery Resources Research Center, Tokyo, pp. 13-30.

Okamoto, S. et al. (2025) Stock assessment and evaluation for Japanese common squid (winter-spawning cohort) (fiscal year 2025). *Marine fisheries stock assessment and evaluation for Japanese waters*. Japan Fisheries Agency and Japan Fisheries Research and Education Agency, Tokyo, 74 pp. https://www.fra.go.jp/shigen/fisheries_resources/meeting/ stock_assessment_meeting/2025/files/sa2025-sc16/fra-sa2025-sc16-01.pdf. Accessed on 12 February 2026 [In Japanese].

Polovina, J. J. et al. (2001) The transition zone chlorophyll front, a dynamic global feature defining migration and forage habitat for marine resources. *Prog. Oceanogr.*, **49**, 469-483. https://doi.org/10.1016/S0079-6611(01)00036-2.

Roper, C. F. E. et al. (1984) Cephalopods of the world. An annotated and illustrated catalogue of species of interest to fisheries. *FAO Fish. Synop.*, **125**, FAO, Rome, Italy, 277 pp.

Sakai, M. et al. (2006) Swimming behaviour in ommastrephid squid by acoustic pinger – 3D pattern of *Ommastrephes bartramii*. *Nihon Baiorogingu Kenkyūkai Dai 2-kai Shinpojiumu 2006 Yōshi* (*The 2nd Symposium of the Bio-logging Society of Japan, Abstract*), pp. 19-20. [In Japanese].

Sakai, M. et al. (2012) Vertical distribution of neon flying squid determined by biotelemetry. *Suisan Kaiyō Gakkai Sōritsu 50 Shūnen Kinen Taikai* (*Proceedings of the 50th Anniversary Meeting of the Japanese Society of Fisheries Oceanography*), 106 pp. [In Japanese].

Silverman, B. W. (1986) *Density estimation for statistics and data analysis.* Chapman & Hall, London, UK, 175 pp.

Vijai, D. et al. (2015) Effects of temperature on embryonic development and paralarval behavior of the neon flying squid *Ommastrephes bartramii*. *Mar. Ecol. Prog. Ser.*, **529**, 145-158.

Watanabe, H. et al. (2004) Feeding habits of neon flying squid *Ommastrephes bartramii* in the transitional region of the central North Pacific. *Mar. Ecol. Prog. Ser.*, **266**, 173-184.

Wang, J. et al. (2021) Water temperature at different depths affects the distribution of neon flying squid (*Ommastrephes bartramii*) in the Northwest Pacific Ocean. *Front. Mar. Sci.*, **8**, 741620.

Worton, B. J. (1989) Kernel methods for estimating the utilization distribution in home-range studies. *Ecology*, **70**, 164-168.